9   Models for atmospheric propagation delays

Techniques operated for the realization of the IERS reference systems make use of electromagnetic signals received on the surface of the Earth. During their transit of the atmosphere, the signals experience delays which must be modeled in the analysis software. This chapter presents models for the propagation of optical signals in the troposphere (9.1), for radio signals in the troposphere (9.2) and for radio signals in the ionosphere (9.4). For Doppler techniques which use time-differenced phases as observables, the models presented in this chapter should be time-differenced as well.

9.1   Tropospheric model for optical techniques

The accuracy of satellite and lunar laser ranging (SLR & LLR) is greatly affected by the residual errors in modeling the effect of signal propagation through the troposphere and stratosphere. Although several models for atmospheric correction have been developed, the more traditional approach in LR data analysis uses a model developed in the 1970s (Marini and Murray, 1973). Mendes *et al.* (2002) pointed out some limitations in that model, namely the modeling of the elevation dependence of the zenith atmospheric delay, *i.e.* the mapping function (MF) component of the model. The MFs developed by Mendes *et al.* (2002) represent a significant improvement over the MF in the Marini-Murray model and other known MFs. Of particular interest is the ability of the new MFs to be used in combination with any zenith delay (ZD) model to predict the atmospheric delay in the line-of-sight direction. Subsequently, Mendes and Pavlis (2004) developed a more accurate ZD model, applicable to the range of wavelengths used in modern LR instrumentation. The combined set of the new mapping function and the new ZD model were adopted in October 2006 by the Analysis Working Group of the International Laser Ranging Service (ILRS) as the new standard model to be used for the analysis of LR data starting January 1, 2007. The alternative to correct the atmospheric delay using two-color ranging systems is still at an experimental stage.

9.1.1   Zenith delay models

The atmospheric propagation delay experienced by a laser signal in the zenith direction is defined as

$$d_{atm}^z = 10^{-6} \int_{r_s}^{r_a} N dz = \int_{r_s}^{r_a} (n-1)\, dz, \tag{9.1}$$

or, if we split the zenith delay into hydrostatic (d_h^z) and non-hydrostatic (d_{nh}^z) components,

$$d_{atm}^z = d_h^z + d_{nh}^z = 10^{-6} \int_{r_s}^{r_a} N_h dz + 10^{-6} \int_{r_s}^{r_a} N_{nh} dz, \tag{9.2}$$

where $N = (n-1) \times 10^6$ is the (total) group refractivity of moist air, n is the (total) refractive index of moist air, N_h and N_{nh} are the hydrostatic and the non-hydrostatic components of the refractivity, r_s is the geocentric radius of the laser station, r_a is the geocentric radius of the top of the (neutral) atmosphere, and d_{atm}^z and dz have length units.

In the last few years, the computation of the group refractivity at optical wavelengths has received special attention and, as a consequence, the International Association of Geodesy (IAG) (IUGG, 1999) recommended a new procedure to compute the group refractivity, following Ciddor (1996) and Ciddor and Hill (1999). Based on this procedure, Mendes and Pavlis (2004) derived closed-form expressions to compute the zenith delay. For the hydrostatic component, we have

$$d_h^z = 0.002416579 \frac{f_h(\lambda)}{f_s(\phi, H)} P_s, \tag{9.3}$$

where d_h^z is the zenith hydrostatic delay, in meters, and P_s is the surface barometric pressure, in hPa. The function $f_s(\phi, H)$ is given by

$$f_s(\phi, H) = 1 - 0.00266 \cos 2\phi - 0.00000028H, \tag{9.4}$$

where ϕ is the geodetic latitude of the station and H is the geodetic height of the station in meters [1], $f_h(\lambda)$ is the dispersion equation for the hydrostatic component

$$f_h(\lambda) = 10^{-2} \times \left[k_1^* \frac{(k_0 + \sigma^2)}{(k_0 - \sigma^2)^2} + k_3^* \frac{(k_2 + \sigma^2)}{(k_2 - \sigma^2)^2} \right] C_{CO_2}, \tag{9.5}$$

with $k_0 = 238.0185\ \mu\mathrm{m}^{-2}$, $k_2 = 57.362\ \mu\mathrm{m}^{-2}$, $k_1^* = 19990.975\ \mu\mathrm{m}^{-2}$, and $k_3^* = 579.55174\ \mu\mathrm{m}^{-2}$, σ is the wave number ($\sigma = \lambda^{-1}$, where λ is the wavelength, in μm), $C_{CO_2} = 1 + 0.534 \times 10^{-6}(x_c - 450)$, and x_c is the carbon dioxide (CO_2) content, in ppm. In the conventional formula, a CO_2 content of 375 ppm should be used, in line with the IAG recommendations, thus $C_{CO_2} = 0.99995995$ should be used.

For the non-hydrostatic component, we have:

$$d_{nh}^z = 10^{-4}\left(5.316 f_{nh}(\lambda) - 3.759 f_h(\lambda)\right) \frac{e_s}{f_s(\phi, H)}, \tag{9.6}$$

where d_{nh}^z is the zenith non-hydrostatic delay, in meters, and e_s is the surface water vapor pressure, in hPa. f_{nh} is the dispersion formula for the non-hydrostatic component:

$$f_{nh}(\lambda) = 0.003101\left(\omega_0 + 3\omega_1\sigma^2 + 5\omega_2\sigma^4 + 7\omega_3\sigma^6\right), \tag{9.7}$$

where $\omega_0 = 295.235$, $\omega_1 = 2.6422\ \mu\mathrm{m}^2$, $\omega_2 = -0.032380\ \mu\mathrm{m}^4$, and $\omega_3 = 0.004028\ \mu\mathrm{m}^6$.

The subroutine `FCUL_ZTD_HPA.F` to compute the total zenith delay is available at [2].

From the assessment of the zenith models against ray tracing for the most used wavelengths in LR, it can be concluded that these zenith delay models have overall rms errors for the total zenith delay below 1 mm across the whole frequency spectrum (Mendes and Pavlis, 2003; Mendes and Pavlis, 2004).

9.1.2 Mapping function

Due to the small contribution of water vapor to atmospheric refraction at visible wavelengths, we can consider a single MF for laser ranging. In this case, we have:

$$d_{atm} = d_{atm}^z \cdot m(e), \tag{9.8}$$

where d_{atm}^z is the total zenith propagation delay and $m(e)$ the (total) MF. Mendes *et al.* (2002) derived a MF, named FCULa, based on a truncated form of the continued fraction in terms of $1/sin(e)$ (Marini, 1972), normalized to unity at the zenith

$$m(e) = \frac{1 + \dfrac{a_1}{1 + \dfrac{a_2}{1 + a_3}}}{\sin e + \dfrac{a_1}{\sin e + \dfrac{a_2}{\sin e + a_3}}}. \tag{9.9}$$

Note that the same formula is used for radio techniques, but with different variables, see Equation (9.13). The FCULa MF is based on ray tracing through one full year of radiosonde data from 180 globally distributed stations. It is valid for a

---

[1] originally, Saastamoinen (1972) used orthometric height, however, the formula is insensitive to the difference, so geodetic height can be used instead without loss of accuracy.

[2] ftp://tai.bipm.org/iers/conv2010/chapter9

Table 9.1: Coefficients (a_{ij}) for the FCULa mapping function, see Equation (9.10). Coefficients (a_{i1}) are in C^{-1} and coefficients (a_{i3}) in m^{-1}.

a_{ij}	FCULa
a_{10}	$(12100.8\pm1.9) \times 10^{-7}$
a_{11}	$(1729.5\pm4.3) \times 10^{-9}$
a_{12}	$(319.1\pm3.1) \times 10^{-7}$
a_{13}	$(-1847.8\pm6.5) \times 10^{-11}$
a_{20}	$(30496.5\pm6.6) \times 10^{-7}$
a_{21}	$(234.6\pm1.5) \times 10^{-8}$
a_{22}	$(-103.5\pm1.1) \times 10^{-6}$
a_{23}	$(-185.6\pm2.2) \times 10^{-10}$
a_{30}	$(6877.7\pm1.2) \times 10^{-5}$
a_{31}	$(197.2\pm2.8) \times 10^{-7}$
a_{32}	$(-345.8\pm2.0) \times 10^{-5}$
a_{33}	$(106.0\pm4.2) \times 10^{-9}$

wide range of wavelengths from 0.355 μm to 1.064 μm (Mendes and Pavlis, 2003) and for elevation angles greater than 3 degrees, if we neglect the contribution of horizontal refractivity gradients. The coefficients a_i (i=1,2,3) have the following mathematical formulation:

$$a_i = a_{i0} + a_{i1}t_s + a_{i2}\cos\phi + a_{i3}H, \tag{9.10}$$

where t_s is the temperature at the station in Celsius degrees, H is the geodetic height of the station, in meters, and the coefficients are given in Table 1, see Mendes *et al.* (2002) for details. The subroutine `FCUL_A.F` to compute the FCULa mapping function is available at $<^2>$.

The new mapping functions represent a significant improvement over other mapping functions available and have the advantage of being easily combined with different zenith delay models. The analysis of two years of SLR data from LAGEOS and LAGEOS 2 indicate a clear improvement in the estimated station heights (8% reduction in variance), while the simultaneously adjusted tropospheric zenith delay biases were all consistent with zero (Mendes *et al.*, 2002).

For users who do not have extreme accuracy requirements or do not know the station temperature, the FCULb mapping function, which depends on the station location and the day of the year, has been developed, see Mendes *et al.* (2002) for details. The subroutine `FCUL_B.F` to compute the FCULb mapping function is available at $<^2>$.

9.1.3   Future developments

The accuracy of the new atmospheric delay models are still far from the accuracy required for global climate change studies. The goal as set forth by the International Laser Ranging Service (ILRS) is better than one millimeter. The LR community has been looking into ways to achieve that accuracy. One significant component that is missing from the above models is to account for the effect of horizontal gradients in the atmosphere, an error source that contributes up to 5 cm of delay at low elevation angles. Ranging at low elevation angles improves the de-correlation of errors in the vertical coordinate with errors in the measurement process (biases). Stations thus strive to range as low as possible, thence the need for model improvements.

Global meteorological fields are now becoming more readily accessible, with higher spatio-temporal resolution, better accuracy and more uniform quality. This is primarily due to the availability of satellite observations with global coverage twice daily. Hulley and Pavlis (2007) developed a new technique, and tested it with real data, computing the total atmospheric delay, including horizontal gradients, via

three-dimensional atmospheric ray tracing (3D ART) with meteorological fields from the Atmospheric Infrared Sounder (AIRS). This technique has already been tested and applied to two years of SLR data from LAGEOS 1 and 2, and for ten core, globally-distributed SLR stations. Replacing the atmospheric corrections estimated from the Mendes-Pavlis ZD and MF models with 3D ART resulted in reducing the variance of the SLR range residuals by up to 25% for all the data used in the analysis. As of May 2007, an effort is in progress to establish a service that will compute these corrections for all of the collected SLR and LLR data in the future. Once this service is in place, it is expected that this new approach will be adopted as the standard for SLR and LLR data reductions.

9.2   Tropospheric model for radio techniques

The non-dispersive delay imparted by the atmosphere on a radio signal up to 30 GHz in frequency, which reaches a magnitude of about 2.3 m at sea level, is conveniently divided into "hydrostatic" and "wet" components. The hydrostatic delay is caused by the refractivity of the dry gases (mainly N_2 and O_2) in the troposphere and by most of the nondipole component of the water vapor refractivity. The rest of the water vapor refractivity is responsible for most of the wet delay. The hydrostatic delay component accounts for roughly 90% of the total delay at any given site globally, but can vary between about 80 and 100% depending on location and time of year. It can be accurately computed *a priori* based on reliable surface pressure data using the formula of Saastamoinen (1972) as given by Davis *et al.* (1985):

$$D_{hz} = \frac{[(0.0022768 \pm 0.0000005)]P_0}{f_s(\phi, H)} \qquad (9.11)$$

where D_{hz} is the zenith hydrostatic delay in meters, P_0 is the total atmospheric pressure in hPa (equivalent to millibars) at the antenna reference point (*e.g.* antenna phase center for Global Positioning System, the intersection of the axes of rotation for VLBI [3]), and the function $f_s(\phi, H)$ is given in Equation (9.4).

There is currently no simple method to estimate an accurate *a priori* value for the wet tropospheric delay, although research continues into the use of external monitoring devices (such as water vapor radiometers) for this purpose. So, in most precise applications where sub-decimeter accuracy is sought, the residual delay must usually be estimated with the other geodetic quantities of interest. The estimation is facilitated by a simple parameterization of the tropospheric delay, where the line-of-sight delay, D_L, is expressed as a function of four parameters as follows:

$$D_L = m_h(e)D_{hz} + m_w(e)D_{wz} + m_g(e)[G_N \cos(a) + G_E \sin(a)]. \qquad (9.12)$$

The four parameters in this expression are the zenith hydrostatic delay, D_{hz}, the zenith wet delay, D_{wz}, and a horizontal delay gradient with components G_N and G_E. m_h, m_w and m_g are the hydrostatic, wet, and gradient mapping functions, respectively, and e is the elevation angle of the observation direction in vacuum. a is the azimuth angle in which the signal is received, measured east from north.

Horizontal gradient parameters are needed to account for a systematic component in the N/S direction towards the equator due to the atmospheric bulge (MacMillan and Ma, 1997), which are about -0.5/+0.5 mm at mid-latitudes in the northern and southern hemispheres, respectively. They also capture the effects of random components in both directions due to weather systems. Failing to model gradients in radiometric analyses can lead to systematic errors in the scale of the estimated terrestrial reference frame at the level of about 1 ppb, as well as cause latitude and declination offsets in station and source positions, the latter also depending on the station distribution (Titov, 2004). A mean *a priori* model for the gradients which is based on re-analysis data of the European Centre for Medium-Range Weather

---

[3]In the case of VLBI, provision should be made to account for the actual path of the photons due to the possible altitude variation of the reference point (Sovers and Jacobs, 1996)

Forecasts (ECMWF) is provided by the subroutine `APG.F` available at $<^4>$ and $<^2>$. However, an a priori model cannot replace the (additional) estimation of gradient parameters, if observations at elevation angles below $15°$ are analyzed. In the case of GPS analyses, such low-elevation data could be deweighted because of multipath effects.

Horizontal tropospheric gradients can reach or exceed 1 mm and their estimation was shown by Chen and Herring (1997) and MacMillan (1995) to be beneficial for VLBI, and by Bar-Sever *et al.* (1998) to be beneficial for GPS. Chen and Herring (1997) propose to use $m_g(e) = 1/(\sin e \tan e + 0.0032)$. Unlike other gradient mapping functions this equation is not affected by singularity at very low elevations (below $5°$).

The hydrostatic and wet mapping functions, m_h and m_w, for the neutral atmosphere depend on the vertical distribution of the hydrostatic and wet refractivity above the geodetic sites. With the availability of numerical weather models (NWM) this information can currently be extracted globally with a temporal resolution of six hours (Niell, 2001). Unlike previous mapping functions these are not limited in their accuracy by the use of only surface meteorological data, as in the functions of Ifadis (1986) or in MTT (Herring, 1992), or of the lapse rate and the heights of the isothermal layer and the tropopause as additionally used in the function of Lanyi (1984), nor by the use of average *in situ* properties of the atmosphere, even if validated with radiosonde data, as in NMF (Niell, 1996). The general form of the hydrostatic and wet mapping functions is (Herring, 1992)

$$m_{h,w}(e) = \frac{1 + \dfrac{a}{1 + \dfrac{b}{1 + c}}}{\sin e + \dfrac{a}{\sin e + \dfrac{b}{\sin e + c}}}. \tag{9.13}$$

The Vienna Mapping Function 1 (VMF1) (Boehm *et al.*, 2006a) is based on exact ray traces through the refractivity profiles of a NWM at $3°$ elevation and empirical equations for the b and c coefficients of the continued fraction in Equation (9.13). Niell (2006) compared mapping functions determined from radiosonde data in 1992 with VMF1 and found that the equivalent station height standard deviations are less than 3 mm, which is significantly better than for other mapping functions available. These results are confirmed by VLBI analyses as shown by Boehm *et al.* (2007a) and Tesmer *et al.* (2007), respectively. Thus, VMF1 is recommended for any global application, such as the determination of the terrestrial reference frame and Earth orientation parameters.

At the webpage $<^4>$, the a coefficients of VMF1 as derived from data of the ECMWF are provided with a time interval of 6 hours for the positions of most sites of the International GNSS Service (IGS), the International VLBI Service for Geodesy and Astrometry (IVS), and the International DORIS Service (IDS), as well as on a global $2.5° \times 2.0°$ grid. Kouba (2008) compares results from the grids with VMF1 given at the sites and provides algorithms on how to use the grids.

The Global Mapping Function (GMF) (Boehm *et al.*, 2006b) is an empirical mapping function in the tradition of NMF that can be calculated using only station latitude, longitude (not used by NMF), height, and day of the year. GMF, which is based on spherical harmonics up to degree and order 9, was developed with the goal to be more accurate than NMF and to be consistent with VMF1. Some comparisons of GMF, VMF1 and other MFs with radiosonde data may be found in (Niell, 2006). GMF is easy to implement and can be used when the best accuracy is not required or when VMF1 is not available. The Fortran subroutines `VMF1.F` and `GMF.F` are available at $<^2>$ and $<^4>$.

9.3   Sources for meteorological data

Because 1 mbar pressure error causes an *a priori* delay error of about 2.3 mm at sea level, it is essential to use accurate estimates of meteorological data (Tregoning and

---

[4]http://ggosatm.hg.tuwien.ac.at/DELAY

Herring, 2006). If meteorological instrumentation is not available, meteorological data may be retrieved from a NWM, *e.g.* the ECMWF as provided together with VMF1 at $<^4>$. In both cases adjustments of the pressure should be applied for the height difference between the location of the pressure measurement (from *in situ* instrumentation or from NWM) and the reference point of the space geodesy instrument. Commonly used formulas for the adjustment can be found in (Boehm *et al.*, 2007b). Alternatively, local pressure and temperature estimates could be determined with the empirical model GPT (Boehm *et al.*, 2007b) that has been developed similarly to the GMF, and is provided as a Fortran routine, `GPT.F`, at $<^2>$ and $<^4>$.

9.4   Ionospheric model for radio techniques

Dispersive effects of the ionosphere on the propagation of radio signals are classically accounted for by linear combination of multi-frequency observations. In past years it has been shown that this approach induces errors on the computed time of propagation that can reach 100 ps for GPS due to the fact that higher order dispersive effects are not considered. For wide-band VLBI observations, the induced errors might reach a couple of ps. In this section the estimation of the effect of higher-order neglected ionospheric terms and possible conventional models are summarized for the microwave range, with frequencies from hundreds of MHz to few tens of GHz.

9.4.1   Ionospheric delay dependence on radio signals including higher order terms

The delay $\delta\rho_I$ experienced by the transionospheric electromagnetic signals, travelling from the transmitter T at $\vec{r}_T$ to the receiver R at $\vec{r}_R$, separated by a distance ρ, can be expressed by the integral of the refractive index n along the ray path:

$$\delta\rho_I = \int_{\vec{r}_T}^{\vec{r}_R} c\frac{dl}{v} - \rho = \int_{\vec{r}_T}^{\vec{r}_R} (n-1)dl \tag{9.14}$$

where $c = 299792458$ m/s is the light speed in free space, v is the actual transionospheric signal propagation velocity at the given place and dl is the differential length element.

Effects on carrier phase data

By neglecting the frictional force, assuming that we are in a cold, collisionless, magnetized plasma such as the ionosphere, the refractive index for the carrier phase, n_p, can be expressed by the Appleton expression, for both ordinary (upper sign) and extraordinary (lower sign) waves, see for instance Davies (1990) page 72:

$$n_p^2 = 1 - \frac{X}{1 - \frac{Y_T^2}{2(1-X)} \pm \left[\frac{Y_T^4}{4(1-X)^2} + Y_L^2\right]^{\frac{1}{2}}} \tag{9.15}$$

where

$$X = \frac{\omega_p^2}{\omega^2}, \qquad Y_L = -\frac{\omega_g}{\omega}\cos\theta, \qquad Y_T = -\frac{\omega_g}{\omega}\sin\theta, \tag{9.16}$$

where θ is the angle between the magnetic field $\vec{B}$ and the electromagnetic (EM) propagation direction $\vec{k}$, and where $\omega = 2\pi f$ is the *circular* frequency corresponding to a frequency f. This applies to the carrier circular frequency ω, and to the plasma ω_p and gyro ω_g circular frequencies associated to the free electrons of the ionosphere:

$$\omega_p^2 = \frac{N_e q^2}{m_e \epsilon_0} \qquad \omega_g = \frac{Bq}{m_e} \tag{9.17}$$

where N_e is the number density of free electrons and B is the magnetic field modulus (both depending on time and position along the EM ray), $q \simeq 1.6022 \times 10^{-19}$C is the absolute value of the electron charge, $m_e \simeq 9.1094 \times 10^{-31}$kg is

the electron mass and $\epsilon_0 \simeq 8.8542 \times 10^{-12}$F/m is the electric permittivity in free space (vacuum). Extraordinary waves (lower sign) can be typically associated to right hand polarized EM signals such as those of GPS antennas, and most L and S Band antennas that receive satellite signals.

For signals with frequencies $\omega >> \omega_p$ (and hence $\omega >> \omega_g$) as for GNSS we may expand (9.15) into a second-order Taylor approximation and retain only terms up to f^{-4}, similarly to the approach of Bassiri and Hajj (1993). The result is, see (Datta-Barua *et al.* 2008) for a detailed discussion of several approximation ways adopted by different authors:

$$n_p = 1 - \frac{1}{2}X \pm \frac{1}{2}XY_L - \frac{1}{8}X^2 - \frac{1}{4}X \cdot Y^2(1 + \cos^2\theta) \tag{9.18}$$

where $Y^2 = Y_L^2 + Y_T^2 = \left(\frac{\omega_g}{\omega}\right)^2$ and again upper sign represents ordinary wave, and lower sign represents extraordinary wave.

The following explicit expression for n_p can be obtained for extraordinary EM signals in terms of the main physical constants and parameters, after substituting X, Y_L and Y_T from equations (9.16):

$$n_p = 1 - \frac{q^2}{8\pi^2 m_e \epsilon_0} \cdot \frac{N_e}{f^2} - \frac{q^3}{16\pi^3 m_e^2 \epsilon_0} \cdot \frac{N_e B \cos\theta}{f^3}$$
$$- \frac{q^4}{128\pi^4 m_e^2 \epsilon_0^2} \cdot \frac{N_e^2}{f^4} - \frac{q^4}{64\pi^4 m_e^3 \epsilon_0} \cdot \frac{N_e B^2 (1 + \cos^2\theta)}{f^4} \tag{9.19}$$

Inserting equation (9.19) into (9.14) leads to the following ionospheric dependent terms in the carrier phase, up to third (f^{-4}) order:

$$\delta\rho_{I,p} = -\frac{s_1}{f^2} - \frac{s_2}{f^3} - \frac{s_3}{f^4} \tag{9.20}$$

After substituting the physical constants, m_e, q, ϵ_0, with 5 significant digits the first, second and third order coefficients, s_1, s_2 and s_3, read (note that the International System of Physical Units (SI) is used, e.g. magnetic field is expressed in Tesla):

$$s_1 = 40.309 \int_{\vec{r}_T}^{\vec{r}_R} N_e dl \tag{9.21}$$

$$s_2 = 1.1284 \cdot 10^{12} \int_{\vec{r}_T}^{\vec{r}_R} N_e B \cos\theta dl \tag{9.22}$$

$$s_3 = 812.42 \int_{\vec{r}_T}^{\vec{r}_R} N_e^2 dl + 1.5793 \times 10^{22} \int_{\vec{r}_T}^{\vec{r}_R} N_e B^2 \left(1 + \cos^2\theta\right) dl \tag{9.23}$$

These expressions are fully equivalent for instance to Equations (2) to (5) in Fritsche *et al.* (2005).

It can be seen in the last expressions (9.20) to (9.23) that the ionospheric delay on the carrier phase is negative, indicating an increase of the phase velocity of the EM transionospheric signal propagation.

In order to assess the importance of the different ionospheric terms for $\delta\rho_{I,p}$ in Equation (9.20), we start with the first term, assuming a high value of Slant Total Electron Content (STEC, see Section 9.4.2 for more details) of $S = \int_{\vec{r}_T}^{\vec{r}_R} N_e dl \sim 300 \times 10^{16}$m^{-2}:

$$\delta\rho_{I,p,1} = -\frac{40.309 S}{f^2} \sim -\frac{1.2 \times 10^{20}}{f^2} \tag{9.24}$$

In this case we obtain a first ionospheric order term $\delta\rho_{I,p,1}$ of up to several km of delay for $f \simeq 150$ MHz (negative for the carrier phase), corresponding to the lower frequency of the NIMS satellite system (U.S. Navy Ionospheric Measuring System,

formerly TRANSIT), and of up to several tens of meters for $f = 1575.42$ MHz (L_1 GPS carrier frequency).

The relative importance of the first ($\delta\rho_{I,p,1} = -s_1/f^2$), second ($\delta\rho_{I,p,2} = -s_2/f^3$) and third order terms ($\delta\rho_{I,p,3} = -s_3/f^4$) also depends on the frequency. The higher order terms are increasingly less important for increasing frequencies (e.g. for VLBI frequencies compared to GPS frequencies). Indeed, from Equations (9.20) to (9.23):

$$\frac{\delta\rho_{I,p,2}}{\delta\rho_{I,p,1}} = \frac{2.7994 \times 10^{10}}{f} \cdot \frac{\int_{\vec{r}_T}^{\vec{r}_R} N_e B \cos\theta dl}{\int_{\vec{r}_T}^{\vec{r}_R} N_e dl} \tag{9.25}$$

By taking typical values reflecting the order of magnitude of $|B_0 \cos\theta_0| \simeq 10^4$nT at a given effective height to evaluate both integrals, the order of magnitude of the ratio of second to first order ionospheric term can be approximated by:

$$\frac{\delta\rho_{I,p,2}}{\delta\rho_{I,p,1}} \simeq \frac{2.7994 \times 10^{10}}{f}|B_0 \cos\theta_0| \sim \frac{2.8 \times 10^5}{f} \tag{9.26}$$

The value of $\delta\rho_{I,p,2}$ is thus typically only 1% of that of $\delta\rho_{I,p,1}$ for $f \simeq 150$ MHz (NIMS), and only 0.1% for $f = 1575.42$ MHz (GPS L_1 carrier).

Similarly, the order of magnitude of the relative value between third and second order ionospheric terms can be estimated as:

$$\frac{\delta\rho_{I,p,3}}{\delta\rho_{I,p,2}} = \frac{7.1998 \times 10^{-10}}{f} \cdot \frac{\int_{\vec{r}_T}^{\vec{r}_R} N_e^2 dl}{\int_{\vec{r}_T}^{\vec{r}_R} N_e B \cos\theta dl} + \frac{1.3996 \times 10^{10}}{f} \cdot \frac{\int_{\vec{r}_T}^{\vec{r}_R} N_e B^2 \left(1 + \cos^2\theta\right) dl}{\int_{\vec{r}_T}^{\vec{r}_R} N_e B \cos\theta dl} \tag{9.27}$$

Considering the typical values used above reflecting order of magnitude of $|B_0 \cos\theta_0| \simeq 10^4$nT at a given effective height to evaluate the integrals, an intermediate angle of $\theta_0 = 45$ deg, and taking $N_0 \simeq 10^{12}$m^{-3} a raw order of magnitude value of effective electron density fulfilling $N_0 \cdot \int_{\vec{r}_T}^{\vec{r}_R} N_e dl = \int_{\vec{r}_T}^{\vec{r}_R} N_e^2 dl$, we get the following relative order of magnitude value between third and second order ionospheric terms:

$$\frac{\delta\rho_{I,p,3}}{\delta\rho_{I,p,2}} \simeq \frac{1}{f}\left(7.1998 \times 10^{-10}\frac{N_0}{|B_0 \cos\theta_0|} + 1.3996 \times 10^{10} \cdot \frac{3}{2}|B_0 \cos\theta_0|\right)$$
$$\sim \frac{7.2 \times 10^7 + 2.1 \times 10^5}{f} \tag{9.28}$$

The order of magnitude of the ratio between third and second order ionospheric terms can thus be as high as about 50% for NIMS frequency $f \simeq 150$ MHz but less than 10% for $f = 1575.42$ MHz, the L_1 GPS carrier frequency.

Another conclusion from this approximation is that the second integral in (9.23) can typically be neglected compared to the first integral depending only on the electron density, as it is typically two orders of magnitude smaller, see Equation (9.28):

$$s_3 \simeq 812 \int_{\vec{r}_T}^{\vec{r}_R} N_e^2 dl \tag{9.29}$$

Finally, in order to show that third order ionospheric approximation should be adequate for most of the radio astronomic-geodetic techniques, we can consider the fourth order term $\delta\rho_{I,p,4}$ in the carrier phase delay. It can be deduced in a similar way as the first to third order terms, but now keeping the terms f^{-5} in the Taylor expansion of Equation (9.15) in the corresponding fourth order term $\delta n_{p,4}$ of the carrier phase ionospheric refraction index term

$$\delta n_{p,4} = -\frac{1}{2}XY_L\left(\frac{X}{2} + Y^2\left[1 + \frac{1}{8}\sin^2\theta\tan^2\theta\right]\right) \tag{9.30}$$

which is expressed with the same notation as in the previous expressions. Using Equations (9.16) and (9.17) as well as Equation (9.14), the fourth order ionospheric term in delay can be expressed as:

$$\delta\rho_{I,p,4} = -\frac{s_4}{f^5} \tag{9.31}$$

where

$$s_4 = \frac{q^5}{128\pi^5 m_e{}^3\epsilon_0{}^2} \int_{\vec{r}_T}^{\vec{r}_R} N_e^2 B\cos\theta dl + \frac{q^5}{64\pi^5 m_e{}^4\epsilon_0} \int_{\vec{r}_T}^{\vec{r}_R} N_e B^3 f(\theta) dl \tag{9.32}$$

and where $f(\theta) = \cos\theta \left(1 + \frac{1}{8}\sin^2\theta\tan^2\theta\right)$. Substituting the values of the constants we get:

$$s_4 = 4.5481 \times 10^{13} \int_{\vec{r}_T}^{\vec{r}_R} N_e^2 B\cos\theta dl + 8.8413 \times 10^{32} \int_{\vec{r}_T}^{\vec{r}_R} N_e B^3 f(\theta) dl \tag{9.33}$$

Taking into account Equations (9.31), (9.33), (9.20) and (9.29), the ratio between the fourth and third ionospheric order terms can be written as:

$$\frac{\delta\rho_{I,p,4}}{\delta\rho_{I,p,3}} = \frac{1}{f}\left(5.5982 \times 10^{10} \frac{\int_{\vec{r}_T}^{\vec{r}_R} N_e^2 B\cos\theta dl}{\int_{\vec{r}_T}^{\vec{r}_R} N_e^2 dl} + 1.0883 \times 10^{30} \frac{\int_{\vec{r}_T}^{\vec{r}_R} N_e B^3 f(\theta) dl}{\int_{\vec{r}_R} N_e^2 dl}\right) \tag{9.34}$$

Taking into account the same approximations and typical values than before, the ratio can be expressed as:

$$\frac{\delta\rho_{I,p,4}}{\delta\rho_{I,p,3}} \simeq \frac{1}{f}\left(5.6 \times 10^{10} |B_0\cos\theta_0| + 1.1 \times 10^{30} \frac{|B_0\cos\theta_0|^3 f(\theta_0)}{N_0|\cos^3\theta_0|}\right)$$

$$\sim \frac{1}{f}\left(5.6 \times 10^5 + 2.3 \times 10^3\right) \tag{9.35}$$

According to this expression the fourth order ionospheric term is only 1% of the third order term for $f \simeq 150$ MHz (NIMS) and less than 0.1% for the L1 GPS carrier at $f = 1575.42$ MHz. Another conclusion from this development is that the fourth order term can be approximated by the first term in Equation (9.33):

$$s_4 \simeq 4.55 \times 10^{13} \int_{\vec{r}_T}^{\vec{r}_R} N_e^2 B\cos\theta dl \tag{9.36}$$

Table 9.2 provides delays corresponding to ionospheric terms of different order and different frequencies of interest in radio astronomic-geodetic research, with the same approximations and particular values as above ($|B_0\cos\theta_0| \sim 10^4 nT$, $N_0 \sim 10^{12}m^{-3}$ and $S \sim 3 \times 10^{18}m^{-2}$). It can be seen, taking as significant threshold the delay value of 1mm, that:

- The first order ionospheric term, as expected, is significant for all the considered frequencies.

- The second order ionospheric term should be taken into account for all the frequencies, except for the high VLBI frequency and those used for Ku band time transfer.

- The third order ionospheric term should be taken into account in NIMS and DORIS low frequencies. It is at the significance limit for GPS and high DORIS frequencies and can be neglected for VLBI and time transfer Ku band frequencies.

- The fourth order can be neglected, except for the very low NIMS frequency of 150 MHz.

Ray bending effects on geometric path excess and ionospheric delay

Moreover the effect of the curvature (or bending) of the ray in terms of geometric path excess can be considered as an additional correction Δs_3 (typically up to few millimeters at low elevation for GPS frequencies), appearing as a f^{-4} dependence too, which can be easily added to the s_3 coefficient of Equation (9.47). In

Table 9.2: Delays (in millimeters) corresponding to the first to fourth higher order ionospheric delay terms (in columns) for a representative subset of typical frequencies used in radio astronomy and geodesy: the values are based on typical values of $|B_0 \cos \theta_0| \sim 10^4$ nT, $\theta_0 = \pi/4$, $N_0 = 10^{12} \mathrm{m}^{-3}$ and $S = 3 \times 10^{18} \mathrm{m}^{-2}$ (the values that can be typically neglected –those lower than 1 mm– can be clearly identified by a negative exponent).

f / MHz	Technique	$\delta\rho_{I,p,1}$ / mm	$\delta\rho_{I,p,2}$ / mm	$\delta\rho_{I,p,3}$ / mm	$\delta\rho_{I,p,4}$ / mm
150	NIMS	$-5.3 \cdot 10^6$	$-9.9 \cdot 10^3$	$-4.8 \cdot 10^3$	$-1.8 \cdot 10^1$
400	NIMS / DORIS	$-7.5 \cdot 10^5$	$-5.2 \cdot 10^2$	$-9.4 \cdot 10^1$	$-1.3 \cdot 10^{-1}$
1228	GPS (L2)	$-8.0 \cdot 10^4$	$-1.8 \cdot 10^1$	$-1.1 \cdot 10^0$	$-5.0 \cdot 10^{-4}$
1575	GPS (L1)	$-4.8 \cdot 10^4$	$-8.5 \cdot 10^0$	$-3.9 \cdot 10^{-1}$	$-1.4 \cdot 10^{-4}$
2000	DORIS	$-3.0 \cdot 10^4$	$-4.2 \cdot 10^0$	$-1.5 \cdot 10^{-1}$	$-4.2 \cdot 10^{-5}$
2300	Low VLBI f.	$-2.3 \cdot 10^4$	$-2.8 \cdot 10^0$	$-8.8 \cdot 10^{-2}$	$-2.2 \cdot 10^{-5}$
8400	High VLBI f.	$-1.7 \cdot 10^3$	$-5.7 \cdot 10^{-2}$	$-4.9 \cdot 10^{-4}$	$-3.3 \cdot 10^{-8}$
12000	Time trans. low Ku f.	$-8.3 \cdot 10^2$	$-1.9 \cdot 10^{-2}$	$-1.1 \cdot 10^{-4}$	$-5.2 \cdot 10^{-9}$
14000	Time trans. high Ku f.	$-6.1 \cdot 10^2$	$-1.2 \cdot 10^{-2}$	$-6.2 \cdot 10^{-5}$	$-2.5 \cdot 10^{-9}$

particular Jakowski *et al.* (1994) derived by ray tracing a simple expression for GPS in which, with the above introduced notation, the coefficient of the f^{-4} term approximating the bending effect is:

$$\Delta s_3 \simeq 2.495 \times 10^8 [(1 - 0.8592 \cos^2 E]^{-1/2} - 1] \cdot \hat{S}^2 \tag{9.37}$$

where E is the spherical elevation, *i.e.* the complement of the zenith angle with respect to the geocenter direction and where the units are <u>not</u> in SI system: the STEC $\hat{S}$ in TECU=$10^{16}\mathrm{m}^{-3}$, the elevation E in degrees and the factor Δs_3 in mm·(MHz)^4. This expression is a particular approximation for GPS of the general results obtained for different frequencies. Details of the typical dependences for other frequencies can be seen in Figure 9.1 for different levels of electron content (8, 40 and 100 TECU) and different elevations (10, 25 and 50 degrees).

Recently Hoque and Jakowski (2008) proposed an update for this expresion taking into account the dependency not only on the STEC but also on the vertical distribution of electron content (by considering the F2 layer scale and maximum ionization heights, see Equation (23) in the given reference). But we retain Equation (9.37) for this document because, as the authors recognize in the same paper, these parameters are not easily available in the practice.

As the ray bending depends on the carrier frequency, an additional effect on the ionospheric correction appears when two different carriers are used, because the STEC differs on the two paths. However, following Hoque and Jakowski (2008) Equation (31), this effect is small (mm level at low elevation).

Effects on code pseudorange data

The corresponding effect can be computed for the code pseudorange measurements, by using the well known relationship between phase and code refractive indices, n_p and n_c respectively, relating the phase velocity with the group (code) velocity, see for instance Davies (1990) page 13:

$$n_c = n_p + f \frac{dn_p}{df} \tag{9.38}$$

A similar relationship holds for the code and carrier phase ionospheric delays, $\delta\rho_{I,c}$ and $\delta\rho_{I,p}$, after introducing Equation (9.38) in Equation (9.14):

$$\delta\rho_{I,c} = \delta\rho_{I,p} + f \frac{d}{df} \delta\rho_{I,p} \tag{9.39}$$

Applying Equation (9.39) to Equation (9.20), the ionospheric effect on code ionospheric delay, up to third order term, is:

$$\delta\rho_{I,c} = \frac{s_1}{f^2} + 2\frac{s_2}{f^3} + 3\frac{s_3}{f^4} \tag{9.40}$$
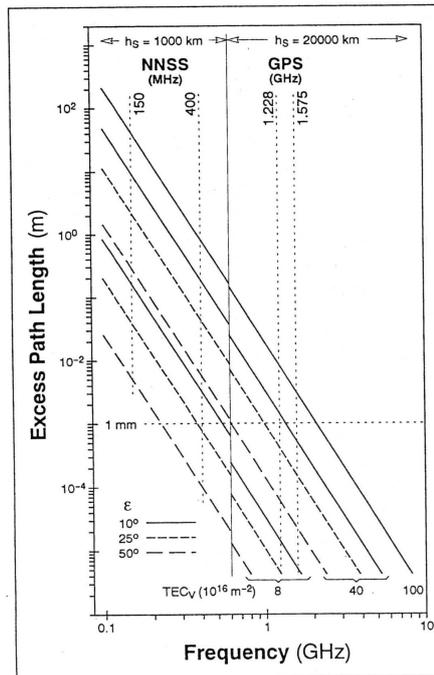
Figure 9.1: Results of ray-tracing calculations concerning the dependency of the excess path length from the frequency of the propagation radio wave. At frequencies below 600 MHz the calculations correspond to a satellite height $h_s = 1000$km (NIMS/NNSS, DORIS) whereas above 600 MHz the calculations correspond to a satellite height $h_s = 20000$km (GPS, GLONASS) [Figure kindly provided by Dr. Norbert Jakowski, see Jakowski *et al.* (1994)]

It can be seen from this relationship, taking into account Equations (9.21), (9.22) and (9.23), that the ionospheric delay on the code pseudorange is positive, associated to a decrease of the EM signal group velocity in the transionospheric propagation.

9.4.2   Correcting the ionospheric effects on code and phase

The most efficient way of correcting the ionospheric effects is by combining simultaneous measurements in k different frequencies, which allows to cancel the ionospheric effects up to order $k - 1$, taking into account Equations (9.20) and (9.40) for carrier phase and code, respectively. A well know example is the case of the actual GPS system with two frequencies, which allows to cancel out the first order ionospheric effect by the so called ionospheric-free combination of observables (see below). And in the future, with Galileo and modernized GPS systems (broadcasting at three frequencies), the full correction can be extended to second order ionospheric terms too.

Correcting the ionospheric term for single frequency users

If the user is only able to gather measurements at a single frequency f, then his main problem is to correct as much as possible (or at least *mitigate*) the first order ionospheric terms in phase and code measurements, $\delta\rho_{I,p,1}$ (9.20) and $\delta\rho_{I,c,1}$ (9.40), which account for more than 99.9% of the total ionospheric delays, as we have shown above. Following (9.21) the first order ionospheric terms are only dependent on the Slant Total Electron Content $S = \int_{\vec{r}_T}^{\vec{r}_R} N_e dl$ and the signal frequency:

$$
\left.
\begin{aligned}
\delta\rho_{I,p,1} &= -40.309 \frac{S}{f^2} \\
\delta\rho_{I,c,1} &= +40.309 \frac{S}{f^2}
\end{aligned}
\right\}
\tag{9.41}
$$

Taking into account this expression, the single frequency users with available phase and code measurements at frequency f_a, and not interested on precise positioning, can use as main observable the so called Graphic combination $G_a = \frac{1}{2} \left(\rho_c^a + \rho_p^a \right)$. In this way the I1 ionospheric delay is completely removed at the price of having an observable with the half part of the code thermal and multipath noise, maintaining as additional unknown the carrier phase ambiguity for each continuous arc of phase data. However the graphic combination can be convenient for real-time users with relatively low requirements of accuracy, in conditions of maximum solar activity and/or low latitude and daylight time or strong ionospheric storms scenarios.

On the other hand, there are different available external sources for the STEC S, which allow to directly correct the single frequency observables. Many of them provide the vertically integrated ionospheric free electron density, the so called Vertical Total Electron Content (VTEC), globally or at least at regional scale.

From the VTEC values (V) corresponding to the observation time, the STEC S can be estimated thanks to a factor approximating the conversion from the vertical to the slant Total Electron Content: the so called *ionospheric mapping function*, M, by $S = M \cdot V$.

Typically a thin shell spherical layer model, at a fixed *effective ionospheric height* h, is applied:

$$M = \frac{1}{\sqrt{1 - \frac{r^2 \cos^2 E}{(r+h)^2}}} \tag{9.42}$$

where r and E are the geocentric distance and ray spherical elevation taken from the user receiver. In the case of IGS the adopted effective height is $h = 450km$. This approximation can introduce significant errors as well, of 5% or more, specially when the 3D nature of the electron density distribution N_e has a larger impact on the integrated (total electron content) values: at low elevation or low latitude observations, see for instance Hernández-Pajares *et al.* (2005). Other better approximations are possible, as Modified Single Mapping Function (Hugentobler *et al.* 2002), variable effective height, see Komjathy and Langley (1996) and Hernández-Pajares *et al.* (2005) or multilayer tomographic model, see for instance Hernández-Pajares *et al.* (2002).

Some common sources of electron content are:

- Global VTEC maps, such as those computed by the International GNSS Service (IGS) <[5]> from a global network of dual-frequency receivers. The user can compute its STEC, S, from interpolating the VTEC maps and applying the corresponding mapping function given by Equation (9.42) with $h = 450km$ in IGS IONEX format, see Schaer *et al.* (1998). The IGS VTEC maps have typically errors of 10 to 20%, see for instance Hernández-Pajares (2004) and Orús *et al.* (2002).

- Predicted VTEC models such as those used by GNSS: Klobuchar model broadcasted in GPS navigation message, or NeQuick <[6]> for the future Galileo system. They can show average errors up to 50% (up to 30% at low latitude, see for instance Orús *et al.* (2002) or Aragón *et al.* (2004). Moreover predicted Global VTEC maps are available from IGS center CODE server <[7]>.

- Regional VTEC models, which provide better accuracy by means of a better temporal and spatial resolution, thanks to the availability of dense networks of permanent receivers (e.g. for Japan, Europe or USA).

- Empirical standard models of the Ionosphere, based on all available data sources, such as the International Reference Ionosphere (IRI, Bilitza 1990) available at <[8]> or PIM (Daniell *et al.* 1995) available at <[9]>. If they

---

[5]ftp://cddisa.gsfc.nasa.gov/pub/gps/products/ionex/
[6]http://www.itu.int/ITU-R/study-groups/software/rsg3-p531-electron-density.zip
[7]ftp://ftp.unibe.ch/aiub/CODE
[8]http://modelweb.gsfc.nasa.gov/ionos/iri.html
[9]http://www.cpi.com/products/pim/pim.html

are adjusted to the actual conditions by means of one or several parameters, such as the Sun Spot Number (Bilitza *et al.* 1999), these empirical models can provide at least similar performance than predicted VTEC models for GNSS. Otherwise the performance can be poor, depending on the region and time.

Correcting the ionospheric term for dual frequency users In case the user is able to gather two simultaneous measurements at two frequencies, f_a and f_b, the situation is much better, because the first order term can be cancelled, elliminating more than 99.9% of the total ionospheric delay. The first-order-ionospheric-free combination $\rho_p^{(1)}$ is defined by the weight factors f_a^2 and $-f_b^2$ as

$$\rho_p^{(1)}(a,b) = \frac{f_a^2 \rho_p^{(a)} - f_b^2 \rho_p^{(b)}}{f_a^2 - f_b^2}. \tag{9.43}$$

If the measurements at the two frequencies are not exactly simultaneous, with a time offset small enough to consider that the electron content does not vary between the two measurements, the linear combination can still be applied but it is necessary to account for the time offset[10].

The first-order-ionospheric-free combination leads to the following new ionospheric dependencies, for carrier phase and code ($\delta\rho_{I,p}^{(1)}$ and $\delta\rho_{I,c}^{(1)}$ respectively), after considering Equations (9.20) and (9.40):

$$\delta\rho_{I,p}^{(1)} = \frac{f_a^2 \delta\rho_{I,p}^{(a)} - f_b^2 \delta\rho_{I,p}^{(b)}}{f_a^2 - f_b^2} = \frac{s_2}{f_a f_b(f_a + f_b)} + \frac{s_3}{f_a^2 f_b^2} \tag{9.44}$$

$$\delta\rho_{I,c}^{(1)} = \frac{f_a^2 \delta\rho_{I,c}^{(a)} - f_b^2 \delta\rho_{I,c}^{(b)}}{f_a^2 - f_b^2} = -\frac{2s_2}{f_a f_b(f_a + f_b)} - \frac{3s_3}{f_a^2 f_b^2} \tag{9.45}$$

where s_2 and s_3 depend on electron density N_e and magnetic field $\vec{B}$, according to expressions (9.22) and (9.29). The following approximations can be done to facilitate the computations:

$$s_2 = 1.1284 \times 10^{12} \int_{\vec{r}_T}^{\vec{r}_R} N_e B \cos\theta dl \simeq 1.1284 \times 10^{12} B_p \cos\theta_p \cdot S \tag{9.46}$$

where B_p and θ_p are the magnetic field modulus and projecting angle with respect to the propagation direction, at an effective pierce point p, and S is the integrated electron density, or STEC S. This approximation is used by Kedar *et al.* (2003) and Petrie *et al.* (2010), and in other references cited above.

For this equation, a source of magnetic field is needed, which should be more realistic than the dipolar one, such as the International Magnetic Reference Field (IMRF) available at $<$[11]$>$ or the Comprehensive Model [12] available at $<$[13]$>$, to reduce errors of up to more than 60% in certain regions, see a discussion in Hernández-Pajares *et al.* (2007). Both models are provided as Fortran routines: the IMRF model is provided with a short description of the arguments as the subroutine igrf10syn in the file igrf10.f at $<$[11]$>$. The Comprehensive Model CM4 is provided with a complete description of the arguments as cm4field.f at $<$[13]$>$.

The third order coefficient can be approximated in terms of the maximum electron density along the ray path N_m:

$$s_3 \simeq 812 \int_{\vec{r}_T}^{\vec{r}_R} N_e^2 dl \simeq 812 \eta N_m S \tag{9.47}$$

---

[10]For example, in some of the Doris instruments, the difference between the two measurement times t_a and t_b can reach 20 microseconds. In this case, it can be shown (Mercier, 2009) that it is sufficient to consider that the linear combination (9.43) should be considered as a measurement taken at the epoch $t^{(1)} = (f_a^2 t_a - f_b^2 t_b)/(f_a^2 - f_b^2)$.

[11]http://www.ngdc.noaa.gov/IAGA/vmod/igrf.html

[12]This model provides different components of the magnetic field besides the main field generated by sources inside the Earth. The external field is caused by charged particle currents in the space around it, primarily in the ionosphere. A calculation of the contribution of these currents to the total magnetic field within the ionosphere has suggested that it is almost two orders of magnitude smaller than that of the main field there, even under geomagnetic storm conditions. If so, the external field can be neglected when computing the second order ionospheric correction.

[13]http://core2.gsfc.nasa.gov/CM/

We may take $\eta \simeq 0.66$ and N_m can be expressed as function of the slab thickness H (which can be modelled as function on the latitude and local time) and the VTEC V, see more details in Fritsche *et al.* (2005) and references therein.

These expressions typically lead for GPS to values of up to few centimeters for the second order ionospheric correction: for instance $\delta\rho_{I,p}^{(1)} \simeq 2$ cm for a given observation with high STEC values (such as $S \simeq 300$ TECU $= 3 \times 10^{18}$ m^{-3}) and magnetic field projection of $B\cos\theta \simeq 3 \times 10^4 nT$.

Moreover the geometric path excess produced by the ray curvature (or bending) can be considered as an additional term depending on f^{-4}, for instance using expression (9.37).

Then, to evaluate $\delta\rho_{I,p}^{(1)}$ and $\delta\rho_{I,c}^{(1)}$ we need as well an STEC source for S, as in the case of single frequency users (see previous subsection). In this case, the double frequency measurements can be used, to provide a direct estimate of S, from the first order term which contains more than 99.9% of it. For instance in GPS S can be estimated from the ionospheric (geometry-free) combination of carrier phases $L_I = L_1 - L_2$ and codes $P_I = P_2 - P_1$, where L_i and P_i are the carrier phase and code measurements for carrier frequency f_i, in length units. Indeed, writing $L_I{}^{14}$ and P_I in terms of the corresponding B_I term (which includes the carrier phase ambiguity and the interfrequency phase biases) and interfrequency delay code biases (DCBs) for receiver and transmitter D and D':

$$L_I = \alpha S + B_I, \qquad P_I = \alpha S + D + D', \qquad (9.48)$$

where $\alpha = 40.309 \cdot (f_2^{-2} - f_1^{-2}) \simeq 1.05 \cdot 10^{-17}$m^3, the STEC S can be estimated as $S = (L_I - <L_I - P_I> - D - D')/\alpha$, where $< \cdot >$ is the average along a carrier phase continuous arc of transmitter-receiver data with no phase cycle-slips. This way of computing the STEC has certain advantages, specially when no external sources of STEC are available (such as in real-time conditions) or at low latitudes and elevations, see Hernández-Pajares *et al.* (2007) for corresponding discussion.

Equations (9.44) to (9.47), with an adequate source of STEC and magnetic field (see above) provide a conventional method to correct the ionospheric higher order terms for dual frequency users.

An alternative approach to correcting the GPS measurements is to apply the second order ionospheric correction by means of redefining the first-order ionospheric free combination of observables (Brunner and Gu 1991), for instance in terms of the line-of-sight magnetic field projection term [15]. This approach has the disadvantage of producing a time dependent carrier phase bias. More details on pros and cons of different approaches for higher order ionospheric corrections, including regional models such as Hoque and Jakowski (2007), can be found in Hernández-Pajares *et al.* (2008).

In the case of DORIS instruments, the measurements are directly the phase variations between successive epochs (intervals of 7 or 10 seconds). They can be processed using the time-differenced first-order-ionospheric-free combination (9.43). For example, for ionospheric studies, this leads to a differential VTEC. VTEC may be deduced with an iterative process (Fleury and Lassudrie, 1992, Li and Parrot, 2007). For the recent instruments (Jason 2 and after), the undifferenced phase and pseudo-range measurements are also available. The pseudo-range measurements are only used to synchronize the on-board oscillator in order to estimate with a sufficient accuracy the measurement time. The first order ionospheric effect can also be removed here using the corresponding combination. For higher order terms, it possible to use as corrections for Doppler the time differences of those for the carrier phase, calculated using the equations for phase given above. But some caution is necessary for DORIS, where the second order effect on the equivalent

---

[14]The wind-up or transmitter-to-receiver antennas rotation angle, is not explicitly written here due its typical small amount -up to less than about 1% of STEC in GPS for example-.

[15]From Equation (9.48) and the definition of the first-order ionospheric free combination of carrier phases $L_c \equiv (f_1^2 L_1 - f_2^2 L_2)/(f_1^2 - f_2^2) = \rho^\star + B_c$ (where $\rho^\star$ contains the frequency independent terms –including geometric distance, clock errors and tropospheric delay– and B_c the carrier phase bias), an apparently first and second order iono free combination of carrier phases can be easily derived $L_c' = \rho^\star + B_c'$, where $L_c' = L_c - s_2 L_I/(f_1 f_2 (f_1 + f_2))$ and $B_c' = B_c - s_2 B_I/(f_1 f_2 (f_1 + f_2))$ are the new combination of observables and time-varying carrier phase bias, respectively.

carrier phase is several times larger than for GPS, on account of the different choice of frequencies. The errors made in the phase correction, and therefore, in the time-differenced phase correction, will be larger. It is not necessary to apply these corrections on the code measurements because the required precision for synchronisation is not so high as for phase processing.

Correcting the ionospheric term for multi (three or more)-frequency users

GNSS systems offering simultaneous observations in 3 or more frequencies should be available soon. Thence, in principle, it should be possible to cancel, from these k simultaneous observations of the same transmitter-receiver pair, up to the first $k - 1$ ionospheric order terms.

As an example, and from Equation (9.43) applied to two pairs of three consecutive frequencies (f_a, f_b and f_c), is possible to define a combination of carrier phase observables that is first and second order ionospheric free, $\rho_p^{(2)}$:

$$\rho_p^{(2)} = \frac{f_a f_b (f_a + f_b) \rho_p^{(1)}(a,b) - f_b f_c (f_b + f_c) \rho_p^{(1)}(b,c)}{f_a f_b (f_a + f_b) - f_b f_c (f_b + f_c)} \tag{9.49}$$

And in terms of the basic observables, given by Equation (9.43), it can be written as:

$$\rho_p^{(2)} = \frac{1}{f_a + f_b + f_c} \left(\frac{f_a^3 \rho_p^{(a)}}{(f_a - f_b)(f_a - f_c)} + \frac{f_b^3 \rho_p^{(b)}}{(f_b - f_a)(f_b - f_c)} + \frac{f_c^3 \rho_p^{(c)}}{(f_c - f_a)(f_c - f_b)} \right) \tag{9.50}$$

From here and from Equation (9.44) the following remaining higher order ionospheric dependence can be deduced:

$$\delta\rho_{I,p}^{(2)} = \frac{s_3}{f_a f_c (f_b^2 + f_b [f_a + f_c])} \tag{9.51}$$

A similar definition to Equation (9.49) can be derived for the code observations resulting, by using Equation (9.45), in the following remaining higher order ionospheric dependency:

$$\delta\rho_{I,c}^{(2)} = \frac{-2s_3}{f_a f_c (f_b^2 + f_b [f_a + f_c])} \tag{9.52}$$

However it must be pointed out that the combination significantly increases the measurement noise. Indeed, from Equation (9.50), considering a simple hypothesis of gaussian independent and identical gaussian distribution for the measurement noise at different frequencies, it is easy to show that the increase of measurement noise is very important (e.g. 25x in Galileo E1, E6, E5 frequencies, 34x in GPS L1, L2, L5, 52x in Galileo E1, E5a, E5b).

References

Aragón, A., Orús, R., Amarillo, F., Hernández-Pajares, M., Juan, J. M., and Sanz, J., 2004, "Performance of NeQuick ionospheric predictions compared with different ionospheric data," Navitec04, December 2004, ESTEC/ESA, Noordwijk, The Netherlands.

Bar-Sever, Y. E., Kroger, P. M., and Borjesson, J. A., 1998, "Estimating horizontal gradients of tropospheric path delay with a single GPS receiver," *J. Geophys. Res.*, **103(B3)**, pp. 5019–5035, doi: 10.1029/97JB03534.

Bassiri, S., and Hajj, G., 1993, "High-order ionospheric effects on the global positioning system observables and means of modeling them," *Manuscr. Geod.*, 18, 280–289.

Bilitza, D., 1990, "International reference ionosphere 1990," URSI/COSPAR, NSSDC/WDC-A-R&S 90-22,
http://iri.gsfc.nasa.gov/docs/IRI1990pp0-84.pdf.

Bilitza, D., Hernández-Pajares, M., Juan, J. M., and Sanz, J., 1999, "Comparison between IRI and GPS-IGS derived electron content during 1991-1997," *Phys. Chem. Earth, Part C*, **24(4)**, pp. 311–319, doi: 10.1016/S1464-1917(99)00004-5.

Boehm, J., Werl, B., and Schuh, H., 2006a, "Troposphere mapping functions for GPS and very long baseline interferometry from European Centre for Medium-Range Weather Forecasts operational analysis data," *J. Geophys. Res.*, **111**, B02406, doi:10.1029/2005JB003629.

Boehm, J., Niell, A. E., Tregoning, P., and Schuh, H., 2006b, "Global Mapping Function (GMF): A new empirical mapping function based on numerical weather model data," *Geophys. Res. Lett.*, **33**, L07304, doi:10.1029/2005GL025546.

Boehm, J., Mendes-Cerveira, P. J., Schuh, H., and Tregoning, P., 2007a, "The impact of mapping functions for the neutral atmosphere based on numerical weather models in GPS data analysis," in *Dynamic Planet — Monitoring and Understanding a Dynamic Planet with Geodetic and Oceanographic Tools*, IAG Symposia, **130**, Springer-Verlag, Rizos, C. and Tregoning, P. (eds.), pp. 837–843, doi: 10.1007/978-3-540-49350-1_118.

Boehm, J., Heinkelmann, R., and Schuh, H., 2007b, "Short Note: A global model of pressure and temperature for geodetic applications," *J. Geod.*, **81(10)**, pp. 679–683, doi:10.1007/s00190-007-0135-3.

Brunner, F., and Gu, M., (1991), "An improved model for the dual frequency ionospheric correction of GPS observations," *Manuscr. Geod.*, 16, 205–214.

Chen, G. and Herring, T. A., 1997, "Effects of atmospheric azimuthal asymmetry on the analysis of space geodetic data," *J. Geophys. Res.*, **102(B9)**, pp. 20,489–20,502, doi: 10.1029/97JB01739.

Ciddor, P. E., 1996, "Refractive index of air: New equations for the visible and near infrared," *Applied Optics*, **35(9)**, pp. 1566–1573, doi: 10.1364/AO.35.001566.

Ciddor, P. E. and Hill, R. J., 1999, "Refractive index of air. 2. Group index," *Applied Optics*, **38(9)**, pp. 1663–1667, doi: 10.1364/AO.38.001663.

Daniell, R. E., Brown, L. D., Anderson, D. N., Fox, M. W., Doherty, P. H., Decker, D. T., Sojka, J. J., and Schunk, R. W., 1995, "Parameterized Ionospheric Model: A global ionospheric parameterization based on first principles models," *Radio Sci.*, **30(5)**, pp. 1499–1510, doi: 10.1029/95RS01826.

Datta-Barua, S., Walter, T., Blanch, J., and Enge, P., 2008, "Bounding higher-order ionosphere errors for the dual-frequency GPS user," *Radio Sci.*, 43, RS5010, doi:10.1029/2007RS003772.

Davies, K., 1990, *Ionospheric Radio*, IEE Electromagnetic Waves Series 31, Peter Pergrinus Ltd., London, UK.

Davis, J. L., Herring, T. A., Shapiro, I. I., Rogers, A. E. E., and Elgered, G., 1985, "Geodesy by radio interferometry: effects of atmospheric modeling errors on estimates of baseline length," *Radio Sci.*, **20(6)**, pp. 1593–1607, doi: 10.1029/RS020i006p01593.

Fleury, R., and Lassudrie-Duchesne, P., 1992. "TEC measurements by means of the DORIS Satellite Positioning System," Proceedings of International beacon satellite symposium (URSI-COSPAR), Cambridge , MA, USA, July 6-10, 1992.

Fritsche, M., Dietrich, R., Knöfel, C., Rülke, A., Vey, S., Rothacher, M., and Steigenberger, P., 2005, "Impact of higher-order ionospheric terms on GPS estimates," *Geophys. Res. Lett.*, 32, L23311, doi:10.1029/2005GL024342.

Hernández-Pajares, M., 2004, "IGS Ionosphere WG Status Report: Performance of IGS Ionosphere TEC Maps -Position Paper-," IGS Workshop, Bern, Switzerland, 2004
http://igs.org/igscb/resource/pubs/04_rtberne/Session11_1.pdf.

Hernández-Pajares, M., Juan, J. M., Sanz, J., and Colombo, O. L., 2002, "Improving the real-time ionospheric determination from GPS sites at very long distances over the equator," *J. Geophys. Res.*, **107(A10)**, 1296, doi:10.1029/2001JA009203.

Hernández-Pajares, M., Juan, J. M., and Sanz, J., 2005, "Towards a more realistic mapping function," A: XXVIII General Assembly of URSI. International Union of Radio Science, p. 34-38.

Hernández-Pajares, M., Juan, J. M., Sanz, J., and Orús, R., 2007, "Second-order ionospheric term in GPS: Implementation and impact on geodetic estimates," *J. Geophys. Res.*, **112**, B08417, doi:10.1029/2006JB004707.

Hernández-Pajares, M., Fritsche, M., Hoque, M., Jakowski, N., Juan, J. M., Kedar, S., Krankowski, A., Petrie, E., and Sanz, J., 2008, "Methods and other considerations to correct for higher-order ionospheric delay terms in GNSS," IGS Analysis Center Workshop 2008, Miami Beach, Florida, USA, http://www.ngs.noaa.gov/IGSWorkshop2008/docs/Higher_order_iono_terms_IGSWS08_v18.ppt.

Herring, T. A., 1992, "Modeling atmospheric delays in the analysis of space geodetic data," in *Proceedings of refraction of transatmospheric signals in geodesy*, Netherlands Geodetic Commission Series, **36**, The Hague, Netherlands, pp. 157–164, http://www.ncg.knaw.nl/Publicaties/Geodesy/pdf/36DeMunck.pdf.

Hoque, M. M., and Jakowski, N., 2007, "Higher order ionospheric effects in precise GNSS positioning," *J. Geod.*, **81(4)**, pp. 259–268, doi: 10.1007/s00190-006-0106-0.

Hoque, M. M., and Jakowski, N., 2008, "Estimate of higher order ionospheric errors in GNSS positioning," *Radio Sci.*, 43, RS5008, doi:10.1029/2007RS003817.

Hugentobler, U., Schaer, S., Beutler, G., Bock, H., Dach, R., Jäggi, A., Meindl, M., Urschl, C., Mervart, L., Rothacher, M., Wild, U., Wiget, A., Brockmann, E., Ineichen, D., Weber, G., Habrich, H., and Boucher, C., 2002, "CODE IGS Analysis Center Technical Report 2002," (see as well http://aiuws.unibe.ch/ionosphere/mslm.pdf.

Hulley, G. C., and Pavlis E. C., 2007, "A ray-tracing technique for improving Satellite Laser Ranging atmospheric delay corrections, including the effects of horizontal refractivity gradients," *J. Geophys. Res.*, **112**, B06417, doi:10.1029/2006JB004834.

Ifadis, I. I., 1986, "The atmospheric delay of radio waves: modeling the elevation dependence on a global scale," *Technical Report No. 38L*, Chalmers U. of Technology, Göteborg, Sweden.

International Union of Geodesy and Geophysics (IUGG), 1999, "Resolution 3 of the International Association of Geodesy," *Comptes Rendus of the XXII General Assembly*, 19–30 July 1999, Birmingham, pp. 110–111.

Jakowski, N., Porsch, F., and Mayer, G., 1994, "Ionosphere-induced ray-path bending effects in precision satellite positioning systems," *Zeitschrift für Satellitengestützte Positionierung, Navigation und Kommunikation*, 1/94, pp. 6–13.

Kedar, S., Hajj, G. A., Wilson, B. D., and Heflin, M. B., 2003, "The effect of the second order GPS ionospheric correction on receiver positions," *Geophys. Res. Lett.*, **30(16)**, 1829, doi:10.1029/2003GL017639.

Komjathy, A., and Langley, R. B., 1996, "The effect of shell height on high precision ionospheric modelling using GPS," Proceedings of the 1996 IGS Workshop, pp. 193–203, Silver Spring, MD, http://igs.org/igscb/resource/pubs/ac_ws96b.pdf.

Kouba, J., 2008, "Implementation and testing of the gridded Vienna Mapping Function 1 (VMF1)," *J. Geod.*, **82(4-5)**, pp. 193–205, doi:10.1007/s00190-007-0170-0.

Lanyi, G., 1984, "Tropospheric delay effects in radio interferometry," *TDA Progress Report 42-78*, pp. 152–159, http://ipnpr.jpl.nasa.gov/progress_report/ 42-78/78N.PDF; see also *Observation Model and Parameter Partials for the JPL VLBI Parameter Estimation Software 'MASTERFIT'-1987*, 1987, JPL Publication 83-39, Rev. 3, http://hdl.handle.net/2060/19880009139.

Li, F., and Parrot, M., 2007, "Study of the TEC data obtained from the DORIS stations in relation to seismic activity," *Annals Geophys.*, **50(1)**, pp. 39–50.

MacMillan, D. S., 1995, "Atmospheric gradients from very long baseline interferometry observations," *Geophys. Res. Lett.*, **22(9)**, pp. 1041–1044, doi: 10.1029/95GL00887.

MacMillan, D. S., and Ma, C., 1997, "Atmospheric gradients and the VLBI terrestrial and celestial reference frames", *Geophys. Res. Lett.*, **24(4)**, pp. 453–456, doi:10.1029/97GL00143.

Marini, J. W., 1972, "Correction of satellite tracking data for an arbitrary tropospheric profile," *Radio Sci.*, **7(2)**, pp. 223–231, doi: 10.1029/RS007i002p00223.

Marini, J. W. and Murray, C. W., 1973, "Correction of laser range tracking data for atmospheric refraction at elevations above 10 degrees," NASA-TM-X-70555, Goddard Space Flight Center, Greenbelt, MD, http://hdl.handle.net/2060/19740007037.

Mendes, V. B., Prates, G., Pavlis, E. C., Pavlis, D. E., and Langley, R. B., 2002, "Improved mapping functions for atmospheric refraction correction in SLR," *Geophys. Res. Lett.*, **29(10)**, 1414, doi:10.1029/2001GL014394.

Mendes, V. B., and Pavlis, E. C., 2003, "Atmospheric refraction at optical wavelengths: problems and solutions," in *Proceedings of the 13th International Laser Ranging Workshop*, Washington D.C., Noomen, R., Klosko, S., Noll, C., and Pearlman, M. (eds.), NASA/CP-2003-212248, http://cddis.gsfc.nasa.gov/lw13/docs/papers/atmos_mendes_1m.pdf.

Mendes, V. B., and Pavlis, E. C., 2004, "High-accuracy zenith delay prediction at optical wavelengths," *Geophys. Res. Lett.*, **31**, L14602, doi:10.1029/2004GL020308.

Mercier, F., 2009, personal communication (see ftp://tai.bipm.org/iers/conv2010/chapter9/add_info/IonoDoris.pdf).

Niell, A. E., 1996, "Global mapping functions for the atmosphere delay of radio wavelengths," *J. Geophys. Res.*, **101(B2)**, pp. 3227–3246, doi: 10.1029/95JB03048.

Niell, A. E., 2001, "Preliminary evaluation of atmospheric mapping functions based on numerical weather models," *Phys. Chem. Earth, Part A*, **26(6-8)**, pp. 475–480, doi: 10.1016/S1464-1895(01)00087-4.

Niell, A. E., 2006, "Interaction of atmosphere modeling and VLBI analysis strategy," in *IVS 2006 General Meeting Proceedings*, Behrend, D. and Baver, K. (eds.), NASA/CP-2006-214140, pp. 252–256, ftp://ivscc.gsfc.nasa.gov/pub/general-meeting/2006/pdf/niell.pdf.

Orús, R., Hernández-Pajares, M., Juan, J. M., Sanz, J., and Garcia-Fernandez, M., 2002, "Performance of different TEC models to provide GPS ionospheric corrections," *J. Atmos. Sol. Terr. Phys.*, **64(18)**, pp. 2055–2062, doi: 10.1016/S1364-6826(02)00224-9.

Petrie, E. J., King, M. A., Moore, P., and Lavallée, D. A., 2010, "Higher-order ionospheric effects on the GPS reference frames and velocities," *J. Geophys. Res.*, **115(B3)**, B03417, doi: 10.1029/2009jb006677.

Saastamoinen, J., 1972, "Atmospheric correction for the troposphere and stratosphere in radio ranging of satellites," *The Use of Artificial Satellites for Geodesy, Geophysical Monograph Series, 15*, Henriksen, S. W., Mancini, A., Chovitz, B. H. (eds.), pp. 247–251.

Schaer, S., Gurtner, W., and Feltens, J., 1998, "IONEX: The IONosphere Map EXchange Format Version 1," ftp://igscb.jpl.nasa.gov/igscb/data/format/ionex1.ps.

Sovers, O. J., and Jacobs, C. S., 1996, *Observation Model and Parameter Partials for the JPL VLBI Parameter Estimation Software 'MODEST'-1996*, JPL Pub. 83–89, Rev. 6.

Tesmer, V., Boehm, J., Heinkelmann, R., and Schuh, H., 2007, "Effect of different tropospheric mapping functions on the TRF, CRF, and position time series estimated from VLBI," *J. Geod.*, **81(6-8)**, pp. 409–421, doi:10.1007/s00190-006-0126-9.

Titov, O. A., 2004, "Construction of a celestial coordinate reference frame from VLBI data," *Astron. Rep.*, **48(11)**, pp. 941–948, doi:10.1134/1.1822976.

Tregoning, P. and Herring, T. A., 2006, "Impact of a priori zenith hydrostatic delay errors on GPS estimates of station heights and zenith total delays, *Geophys. Res. Lett.*, **33**, L23303, doi:10.1029/2006GL027706.